Atomic structure of glassy $Mg_{60}Cu_{30}Y_{10}$ investigated with EXAFS, x-ray and neutron diffraction, and reverse Monte Carlo simulations

Pál Jóvári,[1] Karel Saksl,[2,3] Nini Pryds,[4] Bente Lebech,[5,6] Nicholas P. Bailey,[7] Anders Mellergård,[8,*] Robert G. Delaplane,[8,†] and Hermann Franz[2]

[1]*Research Institute for Solid State Physics and Optics, Hungarian Academy of Sciences, P.O. Box 49, Budapest H-1525, Hungary*

[2]*HASYLAB am Deutschen Elektronen Synchrotron (DESY), Notkestrasse 85, D-22603 Hamburg, Germany*

[3]*Institute of Materials Research, Slovak Academy of Sciences, Watsonova 47, 043 53 Kosice, Slovak Republic*

[4]*Fuel Cells and Solid State Chemistry Department, Risø National Laboratory, DTU, DK-4000 Roskilde, Denmark*

[5]*Materials Research Department, Risø National Laboratory, DTU, DK-4000 Roskilde, Denmark*

[6]*Niels Bohr Institute, University of Copenhagen, DK-2100, Copenhagen, Denmark*

[7]*DNRF Center "Glass and Time," IMFUFA, The Department of Science, Systems and Models, Roskilde University, Universitetsvej 1, DK-4000 Roskilde, Denmark*

[8]*Studsvik Neutron Research Laboratory, Uppsala University, SE-611 82 Nyköping, Sweden*

(Received 23 April 2007; revised manuscript received 12 July 2007; published 22 August 2007)

Short range order of amorphous $Mg_{60}Cu_{30}Y_{10}$ was investigated by x-ray and neutron diffraction, Cu and Y *K*-edge x-ray absorption fine structure measurements, and the reverse Monte Carlo simulation technique. We found that Mg-Mg and Mg-Cu nearest neighbor distances are very similar to values found in crystalline Mg_2Cu. The Cu-Y coordination number is 1.1 ± 0.2, and the Cu-Y distance is ~4% shorter than the sum of atomic radii, suggesting that attraction between Cu and Y plays an important role in stabilizing the glassy state. Thermal stability and structure evolution upon annealing were also studied by differential scanning calorimetry and *in situ* x-ray powder diffraction. The alloy shows a glass transition and three crystallization events, the first and dominant one at 456 K corresponding to eutectic crystallization of at least three phases: Mg_2Cu and most likely cubic MgY and CuMgY.

DOI: 10.1103/PhysRevB.76.054208 PACS number(s): 61.43.Dq, 61.12.Ld, 61.10.Ht

I. INTRODUCTION

Metallic glasses are disordered materials lacking the long range periodicity of crystals, which often results in unique physical and mechanical properties such as high strength and hardness, excellent corrosion resistance, low magnetic energy loss, and easy shaping and forming ability at elevated temperatures.[1–3] Generally, to maintain the amorphous structure of the molten alloy and avoid crystallization during cooling from the melt to the solid phase, high cooling rates (10^5–10^6 K/s) are required. Therefore, only rather thin (typically 10–50 μm) amorphous layers can be obtained. However, in recent years, new multicomponent systems requiring only modest cooling rates ($< \sim 100$ K/s) to become amorphous have been found. Such materials are referred to as "bulk metallic glasses."

Mg-based bulk metallic glasses have attracted attention due to their high strength to weight ratio and low glass transition temperature.[4] The thermal and mechanical properties of amorphous and partly crystalline $Mg_{60}Cu_{30}Y_{10}$ have been presented recently.[5–7] A particularly interesting property of Mg-based bulk metallic glasses is their excellent microforming ability.[8] In spite of their potential practical interest, little is known about the microscopic structure of Mg-based amorphous alloys. Detailed knowledge about the structure of bulk metallic glasses is not only of pure scientific interest but, if achieved, would open possibilities to better control the properties of these materials.

The development of experimental and computational techniques in the past decade significantly improved our knowledge on the formation and physical properties of metallic glasses. Investigations by high energy x-ray diffraction and x-ray absorption techniques revealed the existence of icosahedral local order in liquid metallic alloys.[9,10] The influence of atomic radii of the components on packing, short and medium range order has also been intensely studied.[11] Models based on the efficient packing of atoms and atomic clusters proved to be successful in the prediction of compositions with high glass forming ability.[12,13]

The aim of this paper is to explore the structure of glassy $Mg_{60}Cu_{30}Y_{10}$. In order to get a reliable structural model, we combined x-ray diffraction (XRD) and neutron diffraction (ND) results with Cu *K*-edge and Y *K*-edge extended x-ray absorption fine structure (EXAFS) measurements. The four experimental data sets were fitted simultaneously in the framework of the reverse Monte Carlo simulation technique.[14,15] The resulting atomic configuration was analyzed in detail in terms of pair and higher order correlations. Thermal stability and structure evolution upon annealing were also investigated by differential scanning calorimetry and temperature dependent x-ray diffraction.

II. EXPERIMENT

Prealloyed ingots, with nominal composition $Mg_{60}Cu_{30}Y_{10}$, were prepared by arc melting mixtures of pure Mg, Cu, and Y (99.99 wt. % each) in a purified argon atmosphere. In order to prevent evaporation of Mg, ingots of $Cu_{75}Y_{25}$ were prepared separately, and an appropriate mixture of $Cu_{75}Y_{25}$ and Mg was then melted several times to ensure homogeneity. From these master ingots, amorphous samples were prepared in two forms:

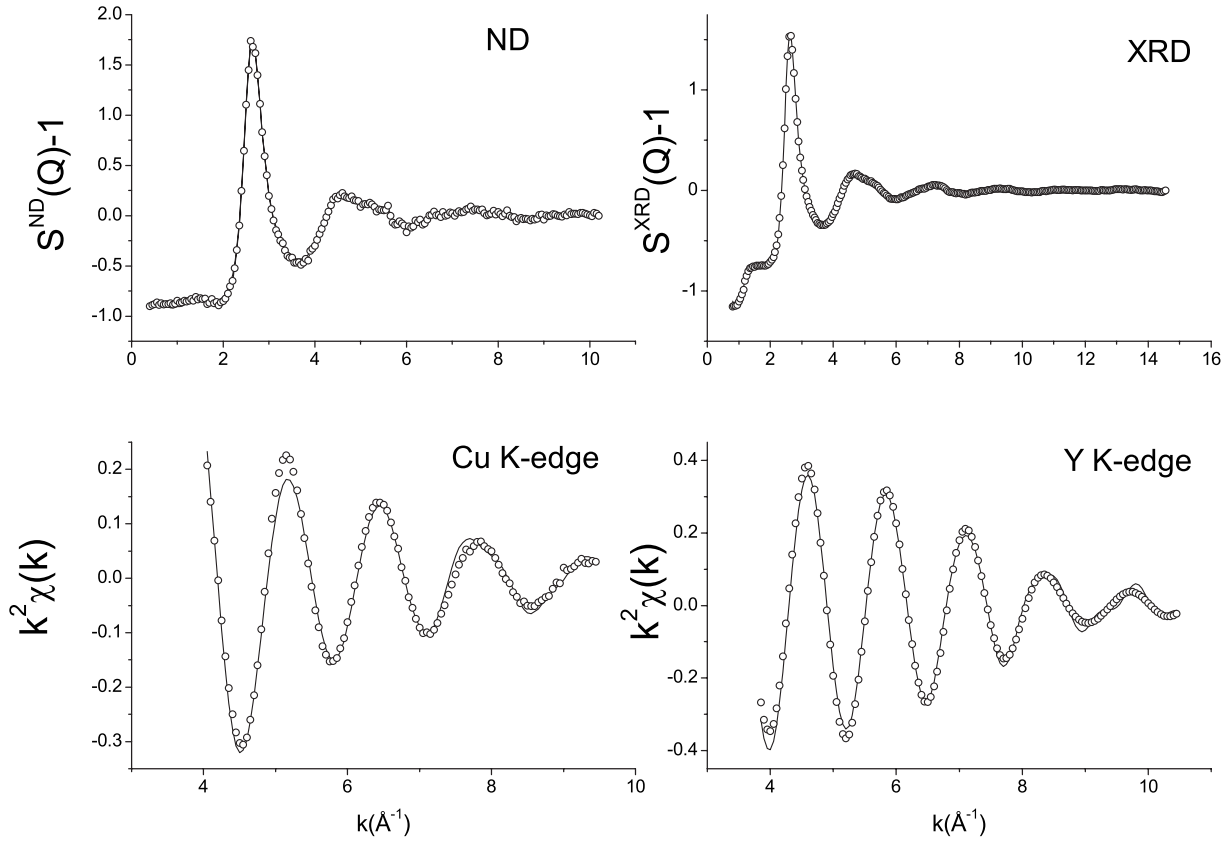

FIG. 1. Experimental (open circle) and model simulation (solid line) of the XRD and ND structure factors and the Cu and Y *K*-edge EXAFS signals of amorphous $Mg_{60}Cu_{30}Y_{10}$.

(i) The alloys were remelted at about 735 K, which is just above their melting point, and then quenched into a cylindrical copper mold under argon atmosphere ($6\times21\times2$ mm^3, used for hard XRD and ND experiments).

(ii) Amorphous ribbons ($\sim3\times0.04$ mm^2 cross section for XRD and EXAFS) were prepared using a single-roller melt-spinning apparatus. The amorphous nature of the samples was confirmed by x-ray and neutron diffraction and by transmission electron microscopy.

It is usually assumed that the density of bulk metallic glasses is only marginally lower than that of corresponding crystalline structures. The mass densities of the amorphous and crystallized phases (measured by the Archimedian method) are 3.541 ± 0.007 g/cm^3 (0.0501 Å^{-3}) and 3.580 ± 0.007 g/cm^3 (0.0507 Å^{-3}), respectively. Combination of the molar volumes of Mg_2Cu and Y [10.97 cm^3 (Ref. 16) and 19.88 cm^3, respectively] gives 3.583 g/cm^3 (0.0508 Å^{-3}) for the density of $Mg_{60}Cu_{30}Y_{10}$. The agreement between this value and the experimentally determined density is remarkable and lends support to the reliability of the experimentally determined densities. A considerably lower value (3.13 g/cm^3) was reported for the amorphous state in an earlier study[17] and adopted later by others.[12,18] In this study, we use 3.541 g/cm^3 as the density of the glassy state.

Differential scanning calorimetric (DSC) measurements were carried out by employing a high sensitivity differential scanning calorimeter (SII-DSC120). The DSC curve was recorded with the specimen held in an inert He atmosphere. The temperature was scanned from room temperature to 600 K with a heating rate of 2 K/min. It was done in order to determine the glass transition temperature (T_g) and the crystallization temperatures (T_X).

XRD measurements were carried out using the BW5 experimental station[19] at the Hamburg Synchrotron Radiation Laboratory, Germany. The energy of the incident beam was 100 keV ($\lambda=0.124$ Å). Samples were illuminated for 200 s by a well collimated incident beam of 1×1 mm^2 cross section. The XRD patterns were recorded using a two-dimensional detector (MAR345, MarResearch). The collected spectra were then integrated into 2θ space by using the FIT2D software.[20] The sample-detector distance, detector orthogonality with respect to the incoming radiation, as well as precise radiation energy was determined by fitting a standard reference LaB_6 sample.[21]

High temperature XRD measurements were carried out from 300 to 625 K at 25 K intervals. In this experiment, a thin walled (10 μm) quartz capillary filled with pieces of ribbon was mounted on a capillary adapter allowing the sample to be kept in a vacuum better than 10^{-5} mbar. Simultaneously, the sample was heated (20 K/min) by an infrared heater designed for *in situ* measurements.[22] The temperature was measured by a thermocouple placed inside the capillary.

Neutron diffraction measurements were performed at room temperature on the SLAD instrument at Studsvik NFL, Sweden.[23] Pieces of ingot were contained in a thin walled vanadium container. The wavelength of the incident radiation

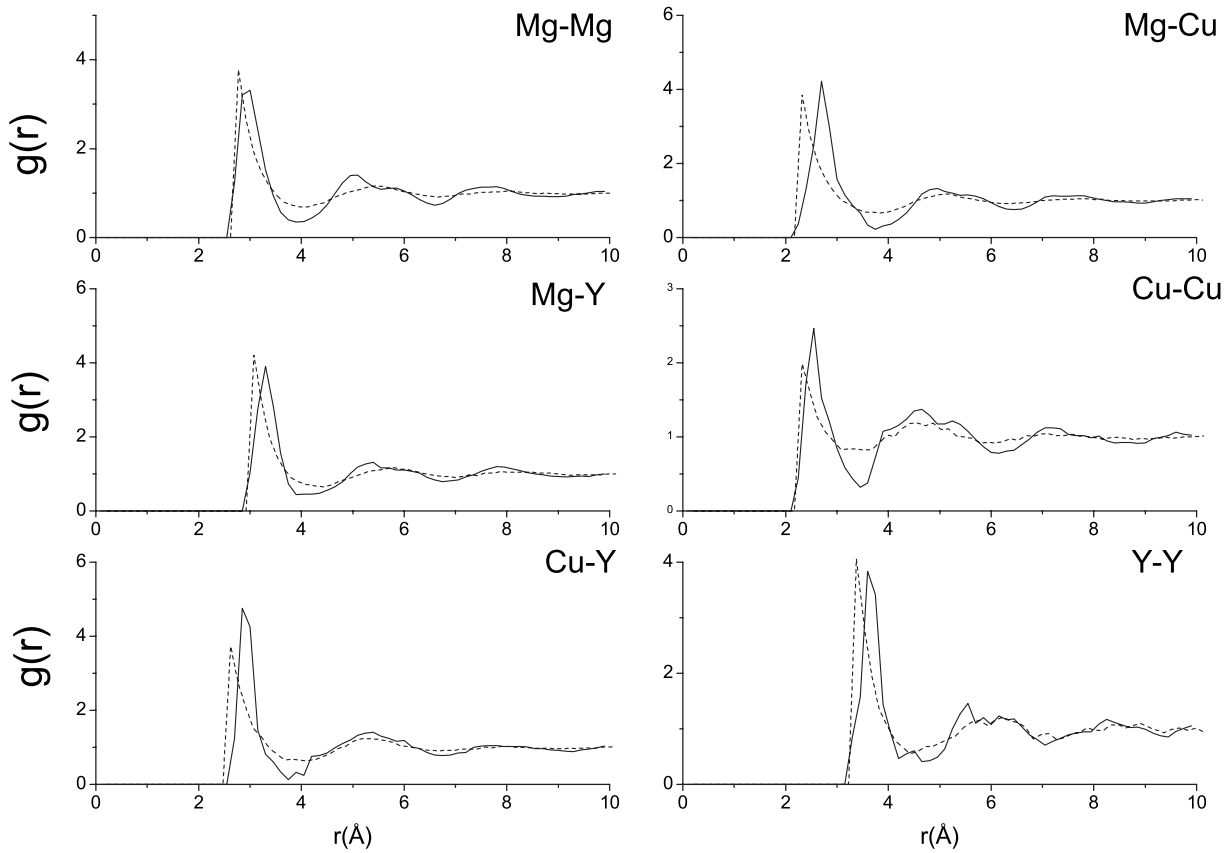

FIG. 2. The partial pair correlation functions $g_{xy}(r)$ obtained from RMC simulation (solid line) and hard sphere model without fitting any experimental data (dashed line).

was 1.1 Å. Additional measurements were made for background, empty container and a solid vanadium rod for normalization. Processing of the raw data was carried out by the CORRECT program package.[24]

EXAFS measurements of amorphous ribbon were performed at HASYLAB at the beam lines X1 (Y K edge) and E4 (Cu K edge). Spectra were collected in transmission mode using fixed exit double-crystal Si(311) and Si (111) monochromators for X1 and E4, respectively. The x-ray intensities were monitored using ionization chambers filled with gases the type and pressure of which were adjusted to the corresponding energies. The energy calibration for Y and Cu was monitored using reference materials measured together with the samples. Experimentally measured x-ray absorption cross sections $\mu(E)$ were analyzed by standard procedures of data reduction using the program VIPER.[25] First, the EXAFS signal $\chi(k)$ was extracted and weighted by k^2. Next, the region where the amplitude of the nonweighted $\chi(k)$ is still significant was Fourier transformed (for details, see Ref. 26). Then the main peak contribution to $\chi(k)$, i.e., the signal from closest atomic neighbors to absorbing atoms, was obtained by filtering and back transforming over an r-space ranges 1.71–3.24 and 1.9–3.66 Å for the Y and Cu K edges, respectively. For the filtering, a Hanning window function with the coefficient $A=0.01$ was used. The signals served later as input for the reverse Monte Carlo (RMC) simulation.

III. REVERSE MONTE CARLO SIMULATION

The reverse Monte Carlo simulation technique offers a framework to generate large three-dimensional models compatible with available structural information. It is used almost exclusively to model diffraction and EXAFS results, but, in principle, any experimental technique can be simulated if the measured signal can be expressed as a function of atomic coordinates. Atomic structures of disordered systems are usually described by partial pair correlation functions (PPCF's) and bond angle distributions (BAD's). In ternary alloys, the structural analysis is complicated by the fact that the number of PPCF's is 6 (in our case, Mg-Mg, Mg-Cu, Mg-Y, Cu-Cu, Cu-Y, and Y-Y), and thus, a detailed structural study requires the combination of experimental information obtained by different techniques (usually diffraction and EXAFS) with prior knowledge (e.g., density and minimum interatomic distances). The RMC simulation technique provides a suitable framework for this task. In this study, we model simultaneously the four measurements: XRD and ND structure factors and the two EXAFS data sets. For details of the simulation, we refer to a recent publication.[27] EXAFS backscattering factors needed to calculate the model EXAFS curves were obtained by the FEFF8.4 program.[28] The simulation boxes contained 20 250 atoms. The following minimum interatomic distances were applied throughout the simulation runs: Mg-Mg, 2.7 Å; Mg-Cu, 2.25 Å; Mg-Y, 3.0 Å; Cu-Cu, 2.25 Å; Cu-Y, 2.55 Å; and Y-Y, 3.3 Å. The initial configura-

TABLE I. Mean interatomic distances (R) and coordination numbers (N) in amorphous $Mg_{60}Cu_{30}Y_{10}$ obtained by RMC simultaneously modeling of the XRD, ND structure factors, and the Cu K-edge and Y K-edge EXAFS data sets.

Pairs	R (Å)	N
Mg-Mg	2.93±0.02	7.5±0.3
Mg-Cu/1	2.72±0.02	1.4±0.2
Mg-Cu/2	3.03±0.05	2.4±0.4
Cu-Mg/1	2.72±0.02	2.7±0.4
Cu-Mg/2	3.03±0.05	4.7±0.8
Mg-Y	3.35±0.02	1.4±0.2
Y-Mg	3.35±0.02	8.3±1.0
Cu-Cu	2.55±0.03	2.0±0.2
Cu-Y	2.94±0.02	1.1±0.2
Y-Cu	2.94±0.02	3.4±0.6
Y-Y	3.69±0.03	1.6±0.2

tion was obtained by a hard sphere simulation satisfying the above constraints.

IV. STRUCTURE OF GLASSY $Mg_{60}Cu_{30}Y_{10}$

A. Pair correlations

Figure 1 shows the comparison of experimental data sets with model curves. The agreement between the experimental and simulated curves is very good for all measurements. The resulting PPCF's can be seen in Fig. 2, where we also show the PPCF's calculated from the initial hard sphere configuration taken as a reference system. The comparison of the two sets of $g(r)$'s may illustrate how the structure of a real metallic glass deviates from a hard sphere system: The first peak positions are shifted to higher r values in comparison with the hard sphere results. The PPCF peak positions and the corresponding coordination numbers are summarized in Table I.

A characteristic feature of the structure of metallic glasses is the shoulder or splitting of the second peak of metal-metal-type PPCF's. In case of $Mg_{60}Cu_{30}Y_{10}$, the shoulder and/or splitting can be found on the Mg-Mg, Mg-Cu, Mg-Y, Cu-Cu, and Y-Y PPCF's. The Mg-Mg peak is at about 2.93 Å, and the corresponding coordination number calculated up to 3.9 Å is 7.5. This value is close to the Mg-Mg distances found in crystalline Mg_2Cu (Table II). The Mg-Cu peak is at 2.72 Å. Integration up to 3.75 Å, the minimum position, gives 3.5 for the Mg-Cu coordination number. This peak is strongly asymmetric and can be decomposed into a Gaussian centered at 2.72 Å and a broader peak at 3.03±0.05 Å. The agreement between the first value and the shortest Mg-Cu distance (2.74 Å) in orthorhombic crystalline Mg_2Cu is remarkable. The Mg-Y peak is at 3.35 Å, and the coordination number is 1.4. The obtained interatomic distance is close to the sum of their nominal atomic radii (3.39 Å). Mg atoms have, on the average, altogether 12.7 neighbors. The Cu-Cu peak position is 2.55±0.03 Å. The corresponding coordination number calculated up to 3.45 Å is 2.0. The Cu-Y peak is at 2.94 Å, and the coordination number is 1.1. This distance is significantly (~5%) shorter than the sum of corresponding atomic radii (3.07 Å) and close to 2.97 Å, the value obtained from orthorhombic YCu_2. These observations suggest a pronounced attraction between Cu and Y in amorphous $Mg_{60}Cu_{30}Y_{10}$. The Cu-X (X=Mg, Cu, or Y) coordination number is 10.5. The Y-Y distance is 3.69 Å, and the coordination number is 1.6. The total number of neighbors around Y is 13.3.

TABLE II. Interatomic distances (r_{wa}) and coordination numbers N in orthorhombic Mg_2Cu. Mg atoms occupy the two nonequivalent 32h Wyckoff sites Mg(1) and Mg(2).

Pairs	r_{wa} (Å)	N
Mg(1)-Mg	3.02	6
Mg(2)-Mg	3.03	6
Mg(1)-Cu	3.49	8
Mg(2)-Cu	2.74	4
Cu-Cu	2.62	2

The efficient cluster packing (ECP) model of metallic glasses[12,13] is based on the dense packing of solute centered atomic clusters. The atoms within such clusters should also be densely packed, which occurs only at specific solute-to-solvent radius ratios. Another important feature of this model is that the central solute atoms are surrounded by solvent atoms only. ECP proved to be especially accurate in the prediction of compositions with good glass forming ability. Coordination numbers around the central solute atoms can also be estimated by the criterion of efficient packing. For the Mg-RE-(Cu, Ni) (RE stands for rare earth) system, the maximum of glass forming ability is about 25 at. % Cu,[29] while ECP gives the highest stability for 24.3 at. % Cu content.[12] According to ECP, the number of Mg atoms around Cu is 10, while Y is surrounded by 15 solvent atoms. These values are in a reasonable agreement with the total number of neighbors

TABLE III. Percentage of the three icosahedral-like local atomic arrangements in the first peaks of partial pair correlation functions obtained from CNA.

	MgMg	MgCu	MgY	CuCu	CuY	YY
555	18%	23%	8%	26%	14%	4%
544	21%	14%	19%	6%	16%	12%
433	23%	26%	21%	32%	24%	20%

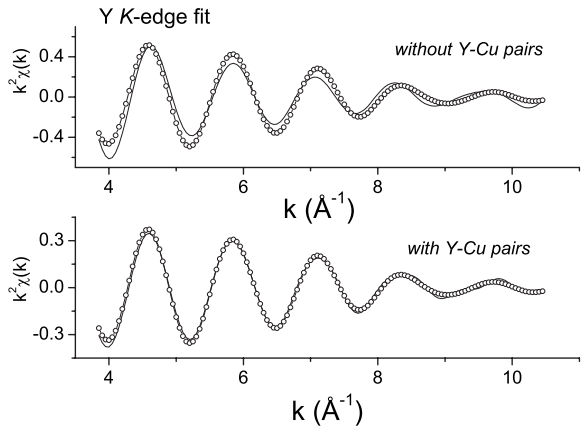

FIG. 3. Fits of Y *K*-edge EXAFS spectrum with and without Y-Cu pairs in the RMC configuration.

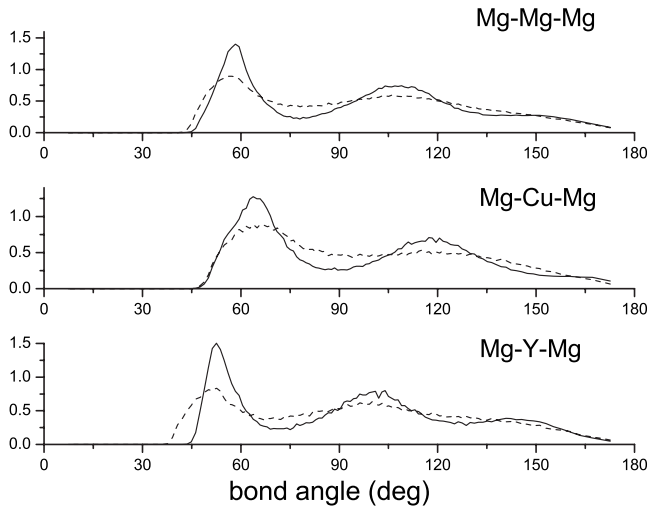

FIG. 4. Selected bond angle distributions calculated from the RMC model (solid lines) and from the reference hard sphere configuration (dashed lines).

of Cu and Y obtained by RMC (10.5 and 13.3, respectively). However, it should be mentioned that according to the RMC simulation results, the number of solute-solute pairs (Cu-Cu, Cu-Y, and Y-Y) is rather high (Table I), which is not emphasized by ECP. The existence of such pairs follows directly from the experimental data. As an illustration, we show the best fit of Y *K*-edge EXAFS measurement that could be achieved by eliminating Cu-Y pairs from the RMC configuration (Fig. 3, upper panel). Another remark is that ECP significantly underestimates the density of $Mg_{60}Cu_{30}Y_{10}$ (2.71 g/cm^3 instead of 3.541 g/cm^3), which strongly suggests that the basic assumptions of ECP may not be valid in case of the Mg-Y-Cu system.

B. Bond angle distributions

Mg-*X*-Mg (X=Mg,Cu,Y) BAD's have also been calculated and compared with those obtained from the reference configuration (Fig. 4). The upper limit of the "bond" has been set to the minimum of the corresponding PPCF's. A pronounced feature in each case is the peak close to 60° that corresponds to the close packing of three equal hard spheres. Besides, the Mg-Mg-Mg BAD shows a broad peak at about 110°. The latter is very close to the second peak of the Mg-Mg-Mg bond angle distribution in crystalline Mg_2Cu ($\sim$106°). No such coincidence can be observed in case of the Mg-Cu-Mg and Mg-Y-Mg BAD's, the peaks of which are at $\sim$120° and at 100° and 150°. The differences between peak positions of the Mg-*X*-Mg BAD's can be qualitatively explained by taking into account the ratio of atomic radii. Cu is the smallest one among the three atomic species. Therefore, the bond angles centered on Cu should shift to higher values in comparison with the Mg-Mg-Mg distribution, as the Cu atom can move closer to the line joining Mg atoms. For the same reason, Mg-Y-Mg bond angles are usually smaller than Mg-Mg-Mg ones.

C. Common neighbor analysis

Common neighbor analysis[30,31] (CNA) is an efficient way of characterizing higher order correlations in disordered systems. In CNA, each pair of atoms is described by three indices: the first gives the number of common neighbors, the second is the number of bonds among common neighbors, while the third index gives the number of bonds in the largest bonded cluster built up of common neighbors. Two atoms are considered as neighbors (or "bonded") if their distance is smaller than the minimum of the corresponding PPCF's. As a consequence, the first index is always zero if the distance of atoms is larger than the sum of the two largest cutoffs. An advantage of this approach is that PPCF's can be decomposed into contributions of pairs with different CNA indices. This way, it can be possible to distinguish between local motifs that cannot be resolved by PPCF's or BAD's.

Simulation studies on liquid and glassy Mg-Cu alloys revealed that the first peak of metal-metal PPCF's are built up mainly from 555-, 544-, and 433-type pairs.[30] In a perfect icosahedron, the central atom forms 555 pairs with all of its 12 neighbors. In this sense, a high number of 555 pairs is a fingerprint of icosahedral local order. 544 and 433 pairs can be obtained by removing a bond or an atom from a 555

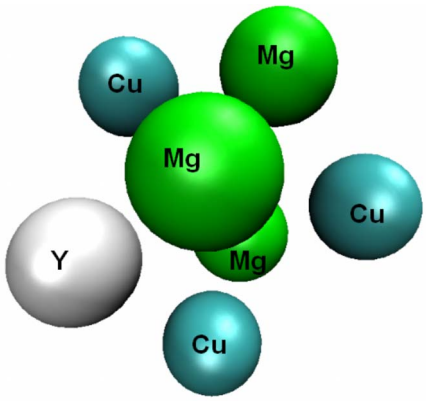

FIG. 5. (Color online) A 555 pair of two Mg atoms (Mg, green; Cu, blue; Y, gray).

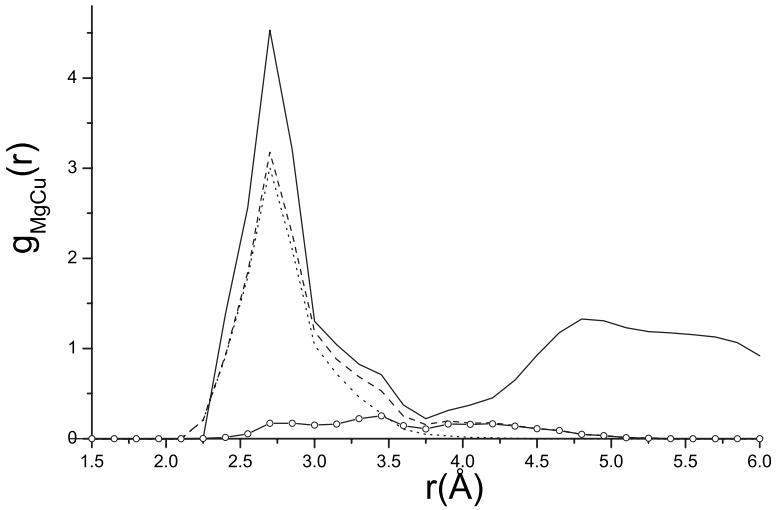

FIG. 6. CNA decomposition of the first peak of $g_{MgCu}(r)$. Solid line, $g_{MgCu}(r)$; dots, sum of the contributions of "icosahedral" 555, 544, and 433 pairs. Line with symbols, sum of 444 and 432 pairs; dashes, sum of icosahedral, 444 and 432 pairs.

arrangement. The contributions of 555, 544, and 433 arrangements to the first peak of the six PPCF's are given in Table III. It can be observed that the relative weight of these icosahedral-like motifs is much higher around Cu and Mg than around Y. A 555 pair of two Mg atoms is shown in Fig. 5.

The average coordination number in glassy Mg_xCu_{1-x} alloys $(0 \leqslant x \leqslant 1)$ is 12.91 ± 0.17 over a wide composition range.[30] The average coordination number in $Mg_{60}Cu_{30}Y_{10}$ is 12.1. The decrease is due to the presence of larger Y atoms. In the binary system, ~70% of the nearest neighbor pairs are in icosahedral-like arrangements (555, 544, or 433). These values show that the local order in $Mg_{65}Cu_{35}$ is quite close to that of crystalline Mg_2Cu in which 80% of atoms (both Cu and Mg) are involved in icosahedral-like arrangements. In $Mg_{60}Cu_{30}Y_{10}$, the percentage of such arrangements is about 63% around Mg and Cu while it is only 48% about Y, which suggests again that icosahedral ordering is stronger around Mg and Cu.

The CNA decomposition of $g_{MgCu}(r)$ revealed that there is no close connection between the asymmetry of the first peak and the more pronounced icosahedral-like ordering around Mg and Cu. Instead, the asymmetry of the peak is caused mainly by several "nonicosahedral" contributions (e.g., 444 and 322) that fill the minimum between the first and second peaks of $g_{MgCu}(r)$. Details can be seen in Fig. 6 where only the sums of most dominant contributions are shown for clarity.

The CNA analysis of the second peaks of PPCF's reveals that the characteristic splitting is due to the separation of 333, 211, and 100 motifs (Fig. 7). Members of a 333 pair sit at the opposite sides of the central hollow formed by the three common neighbors. A 211 arrangement can be considered as the closest in-plane packing of four spheres, while 100 represents three neighboring atoms with a bond angle close to 180°. Thus, 100, 211, and 333 motifs are essentially the closest packing of spheres in one, two, and three dimensions, respectively.

V. THERMAL STABILITY AND CRYSTALLIZATION

Figure 8 shows DSC thermogram of $Mg_{60}Cu_{30}Y_{10}$ recorded at a heating rate of 2 K/min. The profile gives evidence of four transitions, one endothermic at 402 K and

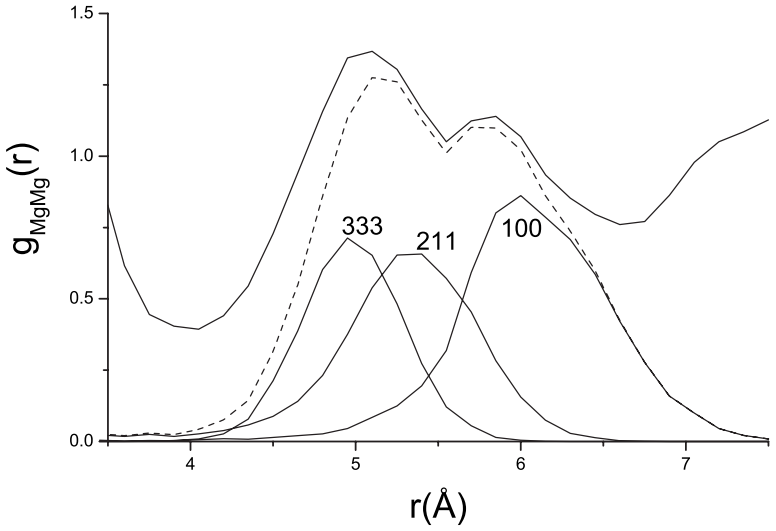

FIG. 7. Common neighbor analysis of the second peak of $g_{MgMg}(r)$.

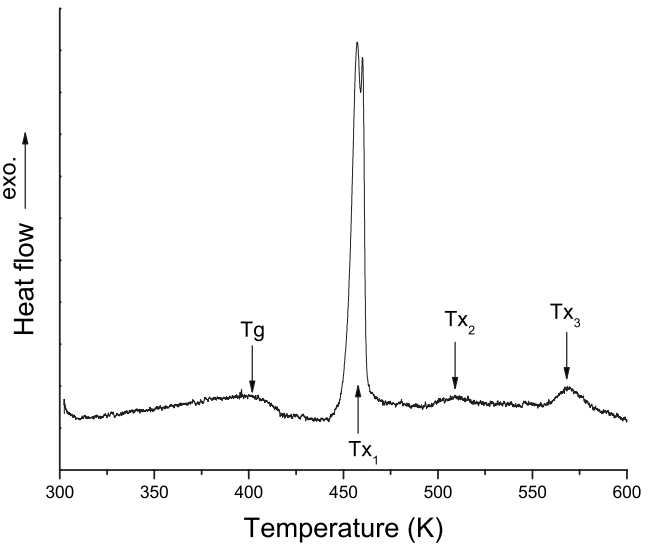

FIG. 8. DSC curves of as-prepared $Mg_{60}Cu_{30}Y_{10}$ at a heating rate of 2 K/min. The transition temperatures are indicated by arrows.

three exothermic reactions at 456, 510, and 568 K. The four transition temperatures are marked by the arrows as T_g, T_{x1}, T_{x2}, and T_{x3} and correspond to the glass transition and the first, second, and third crystallization transitions respectively. The supercooled liquid region of $Mg_{60}Cu_{30}Y_{10}$, defined as the difference between the onset of first exothermic event and T_g, is 43 K wide.

Figure 9 shows XRD patterns from the as-prepared and annealed $Mg_{60}Cu_{30}Y_{10}$ alloy. The as-prepared sample exhibits the diffuse scattering pattern typical for metallic glasses with a maximum at about 3° (2.6 $Å^{-1}$) and a prepeak located around 1.7° (1.5 $Å^{-1}$). The sample at 448 K still looks amorphous, but increasing the temperature by a further 25 K (to 473 K) results in the appearance of Bragg peaks corresponding to the formation of nanocrystalline phases within the amorphous matrix. Besides peaks from orthorhombic Mg_2Cu that were identified in accordance with previous results,[6,7] the XRD pattern shows several Bragg peaks not belonging to this phase. A closer inspection of their position and relative heights admits two *possible* candidates: cubic MgY (symmetry group: $Pm\bar{3}m$; a=3.63 Å) and ternary CuMgY similar to cubic CuMgSn (Symmetric group: $F\bar{4}3m$; a=6.224 Å). Simultaneous crystallization of at least three phases indicates the eutectic rather than primary nature of the first crystallization. XRD intensities change further upon annealing. The pattern at 625 K becomes more crystalline, some peaks change their relative intensities, and some minor peaks appear, but the main motifs do not change. The phase analysis was performed on the sample preannealed at 625 K (temperature above T_{x3}, see Fig. 8) and cooled down to room temperature.

The presence of the cubic phases should be confirmed by transmission electron microscopy and high resolution XRD. The aim of the above remarks is mainly to draw attention to the rather complex crystallization of $Mg_{60}Cu_{30}Y_{10}$.

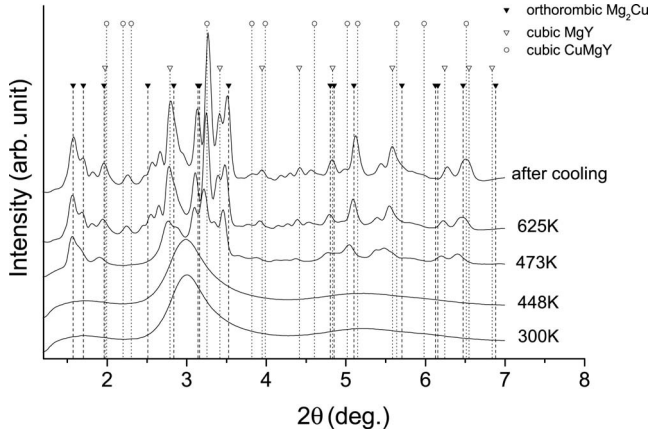

FIG. 9. *In situ* high temperature XRD patterns of $Mg_{60}Cu_{30}Y_{10}$ ribbon samples with marked position of orthorhombic Mg_2Cu (full triangle), cubic MgY (open triangle), and cubic CuMgY (open circle).

VI. CONCLUSIONS

In this paper, we present a structural study on glassy $Mg_{60}Cu_{30}Y_{10}$ prepared by rapid solidification techniques from the melt.

The atomic structure of amorphous $Mg_{60}Cu_{30}Y_{10}$ was characterized by high energy x-ray and neutron diffraction and Cu K-edge and Y K-edge EXAFS. The four data sets were fitted simultaneously by the RMC simulation technique. Pair and higher order correlations in the configuration obtained by RMC were analyzed in detail. Results can be summarized as follows:

(1) The Mg-X (X=Mg,Cu) and Cu-Y distances are significantly shorter than the sum of their Goldschmidt radii and very similar to the corresponding values found in Mg_2Cu and YCu_2 crystalline phases. The Mg-Y distance (3.35 Å) is, on the other hand, close to the sum of the nominal radii of Mg and Y. Mg atoms have, on the average, 12.7 closest neighbors. The total numbers of neighbors around Cu and Y were estimated to 10.5 and 13.3, respectively.

(2) The peaks of Mg-Mg-Mg bond angle distribution are close to the values found in crystalline Mg_2Cu. No such coincidence was observed for the Mg-Cu-Mg and Mg-Y-Mg bond angle distributions.

(3) The common neighbor analysis of the pair distributions revealed that there is a significant contribution of "icosahedral-like" 555, 544, and 433 pairs to each partial pair correlation function. The weight of these pairs is significantly higher for Cu and Mg than for Y.

(4) The short Cu-Y distance suggests a strong attraction between Cu and Y. The Cu-Y coordination number is about 1.1 Thus, the majority of Cu atoms are bonded to Y, which makes the nucleation of binary Mg_2Cu more difficult. *Attraction* between Cu and Y is thus an important factor in stabilizing the glassy structure.

(5) The structural stability upon annealing was investigated by a DSC measurement. The DSC record of the as-prepared sample showed a glass transition at 402 K and three distinct exothermic (crystallization) peaks located at 456, 510, and 568 K. The supercooled liquid region of this alloy,

measured at 2 K/min, is 43 K wide. The first exothermic event corresponds to simultaneous (eutectic) crystallization of at least three phases: Mg_2Cu (positively identified) and most likely cubic MgY and CuMgY.

ACKNOWLEDGMENTS

The neutron scattering experiments were supported by the European Commission under the 6th Framework Programme through the Key Action: Strengthening the European Research Area, Research Infrastructures, Contract No. RII3-CT-2003-505925 P.J. was supported by the OTKA (Hungarian Basic Research Found) Grant No. T048580. K.S. is indebted to the Slovak Grant Agency for Science for financial support (Grant No. 2/7196/27). N.P.B. was supported by the Danish National Research Foundation's (DNRF) Center For Viscous Liquid Dynamics "Glass and Time."

*Present address: Blomstergränd 117, SE-14144 Huddinge, Sweden.

†Present address: Borgdalsgangen 36, SE-61157 Nyköping, Sweden.

[1] A. Inoue, Acta Mater. **48**, 279 (2000).

[2] W. L. Johnson, MRS Bull. **24**, 42 (1999).

[3] A. L. Greer, Science **267**, 1947 (1995).

[4] A. Inoue and T. Masumoto, Mater. Sci. Eng., A **173**, 1 (1993).

[5] Zs. Kovács, A. Castellero, A. L. Greer, J. Lendvai, and M. Baricco, Mater. Sci. Eng., A **387-389**, 1012 (2004).

[6] U. Wolff, N. Pryds, and J. A. Wert, Scr. Mater. **50**, 1385 (2004).

[7] U. Wolff, N. Pryds, E. Johnson, and J. A. Wert, Acta Mater. **52**, 1989 (2004).

[8] N. H. Pryds, Mater. Sci. Eng., A **375-377**, 186 (2004).

[9] K. F. Kelton, G. W. Lee, A. K. Gangopadhyay, R. W. Hyers, T. J. Rathz, J. R. Rogers, M. B. Robinson, and D. S. Robinson, Phys. Rev. Lett. **90**, 195504 (2003).

[10] A. Filipponi, A. Di Cicco, and S. De Panfilis, Phys. Rev. Lett. **83**, 560 (1999).

[11] H. W. Sheng, W. K. Luo, F. M. Alamgir, J. M. Bai, and E. Ma, Nature (London) **439**, 419 (2006).

[12] D. B. Miracle, Acta Mater. **54**, 4317 (2006).

[13] D. B. Miracle, Nat. Mater. **3**, 697 (2004).

[14] R. L. McGreevy and L. Pusztai, Mol. Simul. **1**, 359 (1988).

[15] R. L. McGreevy, J. Phys.: Condens. Matter **13**, R877 (2001).

[16] F. Gingl, P. Selvam, and K. Yvon, Acta Crystallogr., Sect. B: Struct. Sci. **49**, 201 (1993).

[17] A. Inoue, A. Kato, T. Zhang, S. G. Kim, and T. Masumoto, Mater. Trans., JIM **32**, 609 (1991).

[18] N. H. Pryds, M. Eldrup, M. Ohnuma, A. S. Pedersen, J. Hattel, and S. Linderoth, Mater. Trans., JIM **41**, 1435 (2000).

[19] R. Bouchard, D. Hupfeld, T. Lippmann, J. Neuefeind, H.-B. Neumann, H. F. Poulsen, U. Rütt, T. Schmidt, J. R. Schneider, J. Süssenbach, and M. von Zimmermann, J. Synchrotron Radiat. **5**, 90 (1998).

[20] A. P. Hammersley, S. O. Svensson, M. Hanfland M, A. N. Fitch, and D. Häusermann, High Press. Res. **14**, 235 (1996).

[21] NIST Standard Reference Material, SRM 660a.

[22] A. Ehnes, K. Saksl, P. Jóvári, and H. Franz, HASYLAB Annual Report, 2003 (unpublished), available at http://hasyweb.desy.de/science/annual_reports/2003_report/index.html

[23] A. Wannberg, A. Mellergård, P. Zetterström, R. G. Delaplane, M. Grönros, L.-E. Karlsson, and R. L. McGreevy, J. Neutron Res. **8**, 133 (1999).

[24] M. A. Howe and R. L. McGreevy, NFL Studsvik Internal Report, 1996 (unpublished).

[25] K. V. Klementev, J. Phys. D **34**, 209 (2001).

[26] K. V. Klementev, J. Synchrotron Radiat. **8**, 270 (2001).

[27] K. Saksl, P. Jóvári, H. Franz, Q. S. Zeng, J. F. Liu, and J. Z. Jiang, J. Phys.: Condens. Matter **18**, 7579 (2006).

[28] A. L. Ankudinov and J. J. Rehr, Phys. Rev. B **62**, 2437 (2000).

[29] A. Inoue, T. Nakamura, T. Nishiyama, and T. Masumoto, Mater. Trans., JIM **33**, 937 (1992).

[30] N. P. Bailey, J. Schiøtz, and K. W. Jacobsen, Phys. Rev. B **69**, 144205 (2004).

[31] H. Jónsson and H. C. Andersen, Phys. Rev. Lett. **60**, 2295 (1988).